

A Large Sample of Photometric Rotation Periods for FGK Pleiades Stars

J. D. Hartman^{1*}, G. Á. Bakos¹, G. Kovács², R. W. Noyes¹

¹*Harvard-Smithsonian Center for Astrophysics, 60 Garden St., Cambridge, MA 02138, USA*

²*Konkoly Observatory, Budapest, Hungary.*

7 June 2010

ABSTRACT

Using data from the HATNet survey for transiting exoplanets we measure photometric rotation periods for 368 Pleiades stars with $0.4 M_{\odot} \lesssim M \lesssim 1.3 M_{\odot}$. We detect periodic variability for 74% of the cluster members in this mass range that are within our field-of-view, and 93% of the members with $0.7 M_{\odot} \lesssim M \lesssim 1.0 M_{\odot}$. This increases, by a factor of five, the number of Pleiades members with measured periods. Included in our sample are 14 newly identified probable cluster members which have proper motions, photometry, and rotation periods consistent with membership. We compare this data to the rich sample of spectroscopically determined projected equatorial rotation velocities ($v \sin i$) available in the literature for this cluster. For stars with $M \gtrsim 0.85 M_{\odot}$ the rotation periods, $v \sin i$ and radius estimates are consistent with the stars having an isotropic distribution of rotation axes, if a moderate differential rotation law is assumed. For stars with $M \lesssim 0.85 M_{\odot}$ the inferred $\sin i$ values are systematically larger than 1.0. These observations imply that the combination of measured parameters $P(v \sin i)/R$ is too large by $\sim 24\%$ for low-mass stars in this cluster. By comparing our new mass-period relation for the Pleiades to the slightly older cluster M35, we confirm previous indications that the spin-down stalls at ~ 100 Myr for the slowest rotating stars with $0.7 M_{\odot} \lesssim M \lesssim 1.1 M_{\odot}$ – a fact which may indicate that the internal transport of angular momentum is inefficient in slowly rotating solar mass stars.

Key words: stars: rotation, spots, late-type — open clusters and associations: individual: Pleiades — techniques: photometric catalogues

1 INTRODUCTION

Due to its proximity, richness, and age, the Pleiades star cluster ($d \sim 133$ pc, e.g. Soderblom et al. 2005; age ~ 125 Myr, e.g. Stauffer et al. 1998) has served for many years as one of the benchmark clusters in studies of stellar angular momentum evolution. Skumanich (1972) first determined the empirical spin-down relation for solar-type stars ($\omega \propto t^{-1/2}$) by comparing measurements of the projected rotation velocities ($v \sin i$) of solar-mass stars in the Pleiades and the Hyades to the equatorial rotation velocity of the Sun. Since then there have been numerous studies presenting rotation periods and $v \sin i$ values for stars in the Pleiades (see the references given in sections 4.1 and 4.2).

Recently, large samples of stellar photometric rotation periods have been published for a number of open clusters (see for example the summary and references given by

Irwin & Bouvier 2009 for 18 open clusters, together with some new results, not included in their list, for Coma Berenices by Collier Cameron et al. 2009, for NGC 2301 by Sukhbold & Howell 2009, and for M34 by James et al. 2010). These data have enabled theoretical investigations of the angular momentum evolution of low-mass stars (again see the review by Irwin & Bouvier 2009, and also a recent study by Denissenkov et al. 2009), which have led to a number of insights into stellar physics. Observations of very young clusters with ages $\lesssim 10$ Myr can be used to study phenomena such as accretion-driven stellar winds (Matt & Pudritz 2005, 2008a,b) or star-disk-locking (e.g. Königl 1991; Shu et al. 1994). Observations of clusters with ages $\sim 50 - 200$ Myr are essential for constraining the time-scale of coupling between stellar convective and radiative zones (e.g. Bouvier 2008; Denissenkov et al. 2009). Finally, observations of older clusters are important for constraining models of magnetized stellar winds (Kawaler 1988) and for calibrating the rotation-age relation (e.g. Barnes

* E-mail: jhartman@cfa.harvard.edu (JDH)

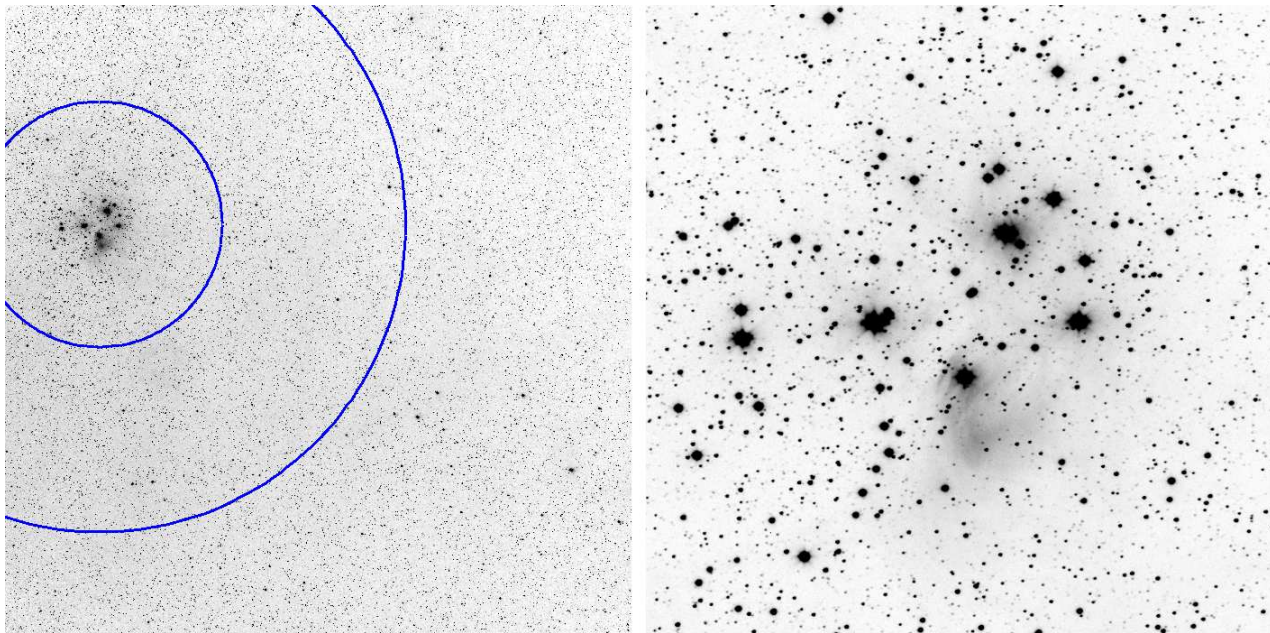


Figure 1. Left: A typical $10.6^\circ \times 10.6^\circ$ HAT-9 image of HATNet field G259 containing the Pleiades cluster. The 2° and 5° radius circles contain 68% and 100% of the candidate cluster members in the catalogue of Stauffer et al. (2007). Right: A $1.5^\circ \times 1.5^\circ$ zoomed-in view of the center of the cluster.

2007; Mamajek & Hillenbrand 2008; Collier Cameron et al. 2009).

Although the comparison of models to the observed rotation period distributions in open clusters has led to a number of insights, these studies are hindered by incompleteness and poorly determined selection effects in the available datasets. These effects may in turn lead to incorrect theoretical inferences. The available photometric rotation periods for the Pleiades, in particular, show evidence of being biased toward short periods (Denissenkov et al. 2009), this is unsurprising since longer period stars generally have lower amplitude variations and also require observations spanning a longer time-base to be detected, moreover apparent variations due to systematic errors in the photometry may dominate on long time-scales; the results to be discussed here do not suffer from this bias because of the long time-base and high precision of our observations. It is only possible to determine whether or not the photometric periods are biased for this cluster because it is fairly unique in having a rich, unbiased sample of $v \sin i$ values in the literature. Given the importance of the Pleiades for the study of stellar angular momentum evolution, an unbiased sample of rotation periods for stars in this cluster would be quite useful.

In this paper we present photometric periods that we associate with rotation periods for 368 Pleiades stars. This increases the number of Pleiades stars with measured periods by a factor of 5, and importantly, it is 93% complete for stars in the mass range $0.7 M_\odot \lesssim M \lesssim 1.0 M_\odot$. For this survey we use data from the Hungarian-made Automated Telescope Network (HATNet Bakos et al. 2004), a project that uses a network of 6 small-aperture, wide-field, fully-automated telescopes to search for transiting exoplanets orbiting bright stars (e.g. Bakos et al. 2010). A similar study of stellar rotation for field K and M dwarf stars using HATNet

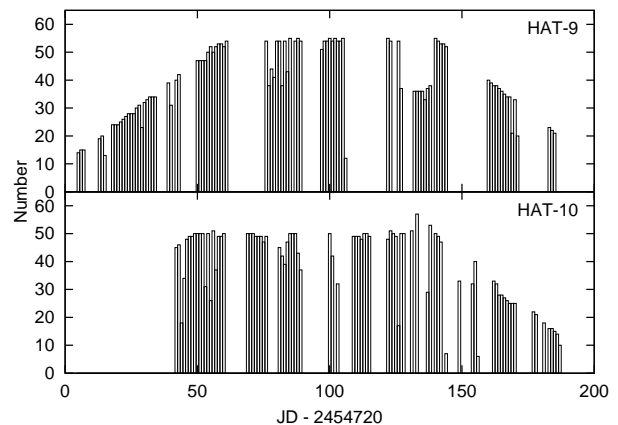


Figure 2. The number of observations of HATNet field G259 obtained on each night with the HAT-9 and HAT-10 instruments.

has been recently presented by our group (Hartman et al. 2009b).

The structure of the paper is as follows: in section 2 we briefly describe the photometric observations and data reduction; in section 3 we select periodic variable stars, estimate the errors on the period, correct the light curves for distortions, present the catalogue of rotation periods, and select new cluster members; in section 4 we compare our data to previous rotation period and $v \sin i$ measurements, and we also compare our results to other open clusters. We summarize the results in section 5.

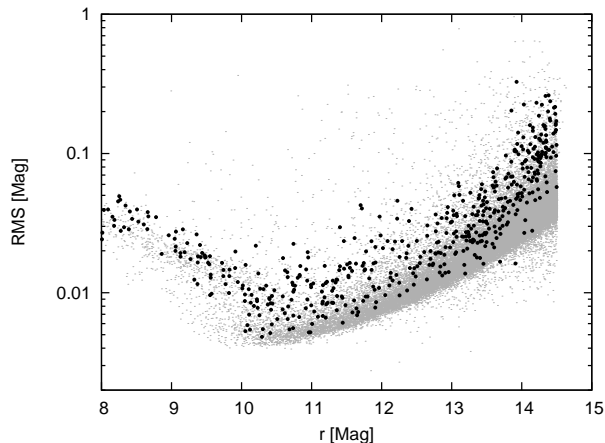


Figure 3. Unbiased RMS (eq. 2) vs. Sloan r magnitude for the EPD/TFA corrected light curves of stars in field G259 (gray-scale points). The dark filled circles show probable Pleiades members (section 3.4). Stars brighter than $r \lesssim 10$ are saturated in a significant fraction of the images.

2 OBSERVATIONAL DATA AND INITIAL REDUCTION

Photometric time-series observations of the Pleiades cluster were obtained between 15 September 2008 and 16 March 2009 using the identical HAT-9 and HAT-10 11 cm aperture robotic telescopes located at Mauna Kea Observatory (MKO) in Hawaii and at Fred L. Whipple Observatory (FLWO) in Arizona respectively. Each telescope used a $4K \times 4K$ CCD and a Sloan r filter to observe a $10.6^\circ \times 10.6^\circ$ field of view (FOV) centered at 03:30:00, 22:30:00 (J2000). The Pleiades are not centered in this field; the field (internally designated as G259) was observed as part of the standard operations of the HATNet transit survey, and was not specifically chosen to observe the cluster. Figure 1 shows a typical image of this field. The images have a pixel scale of $9''$; the full-width at half-maximum (FWHM) of the point-spread function (PSF) is ~ 2.6 pixels ($23''$). A total of 3648 exposures of 5 minutes, taken at 5.5 minute cadence, were obtained with the HAT-9 instrument, while 3138 images with the same exposure time and cadence were obtained with the HAT-10 instrument. Figure 2 shows the temporal distribution of observations obtained with each of these instruments.

The images were calibrated and reduced to light curves using tools developed for the HATNet transit survey (see Pál 2009; Bakos et al. 2004). Briefly, after applying bias, dark current, and twilight sky-flat calibrations in a standard fashion, stars were identified on the images. The star lists were then matched to the Two Micron All-Sky Survey (2MASS; Skrutskie et al. 2006) point source catalogue (PSC) using the methods described by Pál & Bakos (2006) to determine the astrometric solutions for the images. Aperture photometry is then performed at the positions of all 2MASS sources with $r \lesssim 14.5$ transformed to the image coordinate system. For each resulting light curve the median magnitude is fixed to the approximate r magnitude of the source based on the following transformation from the 2MASS J , H and K_S magnitudes (see Bilir et al. 2008, who give transformations from 2MASS magnitudes to Sloan

($g - r$) and ($r - i$) colors; we followed the same procedure to determine a transformation from 2MASS magnitudes to Sloan r magnitude):

$$r = 0.6975 + 2.9782J - 0.8809H - 1.1230K_S. \quad (1)$$

The RMS scatter between the observed and predicted r magnitudes for the stars used to determine this relation is 0.076 mag. For each source, photometry is performed using three apertures of radii 1.45, 1.95 and 2.35 pixels. Following the post-processing routines discussed below, we adopt a single “best” aperture for each light curve. For stars with $r > 13.5$ we take the smallest aperture to minimize sky noise, for brighter stars we adopt the aperture for which the processed light curve has the smallest RMS.

The initial ensemble calibration of the light curves against variations in the flux scale was performed using the method described in section 2.7.3 of (Pál 2009). These light curves are then passed through two routines that filter out systematic variations that are correlated with measureable instrumental parameters or are present in other stars in the field. The first routine, external parameter decorrelation (EPD), decorrelates each light curve against a set of measured instrumental parameters including the shape of the PSF, the sub-pixel position of the star on the image, the zenith angle, the hour angle, the local sky background, and the variance of the background (see Bakos et al. 2010). This decorrelation is done independently on the data from the HAT-9 and HAT-10 telescopes. The procedure is applied assuming that each star has a constant magnitude. For large amplitude variable stars this may distort the signal and may lower the S/N of the detection, however such large amplitude variables will generally still be detectable.

After applying EPD, the light curves are then processed with the Trend-Filtering Algorithm (TFA; Kovács, Bakos & Noyes 2005) which decorrelates each light curve against a representative sample of other light curves from the field. We used 530 template stars ($\sim 8\%$ of the total number of images for the field). In applying the TFA routine we also clip 5σ outliers from the light curves. At this point in the analysis we apply EPD and TFA in signal-recovery mode (i.e. we apply them under the assumption that the signal is constant), once a signal is detected we then apply EPD and TFA in signal-reconstruction mode on the original light curve to obtain an undistorted trend-filtered light curve for the star (see section 3.3). As for EPD, signal-recovery mode TFA may distort the signal and lower the S/N of large amplitude variable stars, though typically the effect is not significant enough to prevent the variable from being selected.

In figure 3 we show the unbiased RMS of the EPD/TFA corrected light curves for all stars in field G259. The unbiased RMS of a light curve is calculated using

$$\text{RMS} = \sqrt{\frac{\sum (m_i - \langle m \rangle)^2}{N - N_P}} \quad (2)$$

where m_i are the individual magnitudes, $\langle m \rangle$ is the average magnitude, N is the number of points in the light curve, and $N_P = 544$ is the number of parameters used in applying EPD/TFA. We mark separately the probable Pleiades members (see section 3.4). Stars with $r \lesssim 10$ are saturated in a significant fraction of the images (due to vignetting the exact magnitude of saturation depends on the

position of the star on the image; it also depends on the sky brightness and transparency which changes from image to image). The unbiased RMS of stars with $r \sim 10$ is ~ 4 mmag. The light curves of Pleiades members generally have greater RMS than those of field stars; this reflects the fact that detectable photometric variability is significantly more common for Pleiades members than it is for field stars (see section 3.4).

3 SEARCH FOR PERIODIC VARIABLES

We use the Lomb-scargle periodogram (Lomb 1976; Scargle 1982; Press & Rybicki 1989) as implemented in the VAR-TOOLS program (Hartman et al. 2008b) to search the light curves for periodic variations. We generate the periodogram for each light curve at a frequency resolution of $0.1/T$ between 0.01 d^{-1} and 10.0 d^{-1} , where T is the time-span of a given light curve. The high-frequency cut-off of 10.0 d^{-1} is adopted as stars are not expected to have rotation periods shorter than this, and expanding the range of the frequency search increases the bandwidth penalty, decreasing the significance of a given detection. We correct the periodogram for red noise by removing any low-order frequency dependence in the mean value of the periodogram and in the RMS of the periodogram. To do this we fit a fifth order polynomial to the periodogram, as well as a fifth order polynomial to the RMS of the periodogram calculated in 100 frequency bins. We then define a new periodogram using

$$p'(\omega) = \frac{\langle \sigma \rangle}{\sigma(\omega)} (p(\omega) - \bar{p}(\omega)) + \langle \bar{p} \rangle \quad (3)$$

where p is the value of the original periodogram at frequency ω , $\sigma(\omega)$ is the polynomial fit to the RMS of the periodogram as a function of frequency, $\bar{p}(\omega)$ is the polynomial fit to the periodogram, and the brackets denote averaging over frequency. We perform the fit using 5- σ iterative clipping, using the model value of $\sigma(\omega)$ in the clipping.

We identify the highest peak in the corrected periodogram p' and determine its S/N using an iterative 5- σ clipping in calculating the RMS of the periodogram. To set the selection threshold we simulate 10000 white noise light curves with the same time sampling as the observations, calculate the red-noise corrected L-S periodogram of each simulation, and determine the S/N of the highest peak in each periodogram using the same procedure as used for the real light curves. Figure 4 shows the false alarm probability (FAP) as a function of S/N determined from the simulations, which we find to be well-fit by a function of the form:

$$\text{FAP} = 1 - (1 - e^{-0.84(S/N+1)})^{1240}. \quad (4)$$

This is similar to the form expected for a normalized L-S periodogram without red-noise correction or clipping (e.g. Press et al. 1992). We adopt a cut-off of $S/N > 16$ which corresponds to a 0.08% FAP. A total of 2236 of the 36,011 stars in the field pass the selection. In section 3.4 below we focus on the stars that are likely to be cluster members. Adopting a lower threshold of $S/N > 13$ (corresponding to a 1% FAP) would increase the total number of selected potential variable stars to 2878.

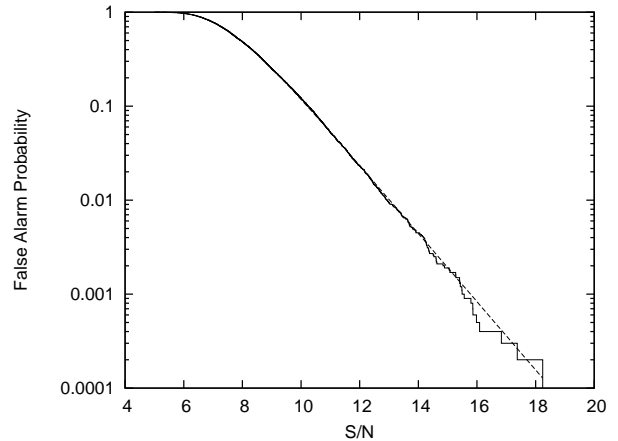


Figure 4. False alarm probability vs. S/N of the peak in the red-noise corrected L-S periodogram. The solid line shows the results from conducting simulations of white noise light curves, the dashed lines shows eq. 4.

3.1 Resolving Aliases

In some cases there is an ambiguity in choosing the correct period from among several possible aliases or harmonics. In general we follow the convention of adopting the highest S/N peak in the red-noise corrected L-S periodogram. We found, however, that often the red-noise correction changes the most significant peak in the periodogram to a high frequency alias $|f_s - f_0|$ of the most significant peak in the uncorrected periodogram, f_0 . Here f_s is the sidereal frequency. In these cases we adopt the period from the uncorrected periodogram. We found that generally the periods from the red-noised corrected periodograms pile-up near 1 day while the periods from the uncorrected periodograms fall along the main period-mass relation (see figure 12).

3.2 Estimation of Period Uncertainties

As discussed by Hartman et al. (2009a), the primary factors that contribute to errors in the measured photometric rotation period are:

Instrumental Effects

- (i) choosing an alias or harmonic of the true period,
- (ii) noise in the photometry together with finite sampling of the light curve,
- (iii) inadequacies in the model used to determine the period (e.g., the light curve is periodic but not sinusoidal),

Physical Effects

- (iv) spot evolution, and
- (v) differential rotation.

The periodogram for a light curve will contain several discrete peaks at harmonics and aliases of the true period. Deciding which peak is the correct one is difficult to do in general. We do not consider this effect in estimating the uncertainties on the measured periods.

The effects (ii)-(iv) listed above all contribute to the spread in the periodogram peak, which reduces the precision with which the position of the peak may be measured. We determine the resulting error in the period by fitting a Gaussian function to the points within $2/T$ of the periodogram peak and measuring the 1σ spread in the position of the peak using the Extended Markov-Chain Monte Carlo technique (see Pál 2009). We set the error for each point in the periodogram equal to the RMS of the full periodogram determined with an iterative 5σ clipping. We also record the standard deviation of the best-fit Gaussian, as this contains information on the spot life-times.

Differential rotation may contribute to the uncertainty in two ways. If there are multiple spot groups at different stellar latitudes, the differing rotation periods for each group will broaden the periodogram peak, and will contribute to the uncertainty in the period as just described. Differential rotation will also lead to a systematic error in determining the rotation period of the star since the degree of differential rotation and the latitude of the dominant spot group are not known, making it impossible to relate the measured period to the period at a reference latitude (such as the equator). If Pleiades stars exhibit solar-like differential rotation (the rotation period increases towards the poles), the measured periods will be systematically longer than the equatorial period. The Sun exhibits differential rotation following

$$P_\beta = P_{\text{EQ}}/(1 - k \sin^2 \beta) \quad (5)$$

where P_β is the rotation period at latitude β , P_{EQ} is the equatorial rotation period, and $k = 0.19$ when using spots to track the rotation (Kitchatinov 2005). For younger, more rapidly rotating stars, the value of k is expected to decrease (Brown et al. 2004). Observations of the $P = 8.77$ d solar-like star κ^1 Ceti by the *Microvariability and Oscillations of Stars (MOST)* satellite bear this theoretical expectation out, finding $k = 0.09$ (Walker et al. 2007). The observations of κ^1 Ceti also indicate that spots on rapidly rotating stars may be found at any latitude; this is in contrast to the Sun where spots are rarely seen with $|\beta| > 30^\circ$. Assuming the dominant spot groups are isotropically distributed on Pleiades stars (i.e. $\sin \beta$ is uniformly distributed), and that these stars exhibit solar-like differential rotation with $k = 0.09$, we expect the measured rotation periods to have a mean value of $1.03P_{\text{EQ}}$, with a standard deviation of $0.03P_{\text{EQ}}$. For $k = 0.19$ the respective values are $1.07P_{\text{EQ}}$ and $0.07P_{\text{EQ}}$. We do not include systematic errors due to differential rotation in the period uncertainties reported in our catalogue.

3.3 Signal Reconstruction with EPD/TFA

Once a period is determined for a star, we obtain a new trend-filtered light curve by running EPD and TFA in signal reconstruction mode (e.g. Kovács, Bakos & Noyes 2005). This correction is important to get an unbiased measurement of the amplitude of photometric variations. To do this, we fit to the pre-EPD light curve (i.e. the light curve has been corrected for ensemble variations in the flux scale, but has not had any other filtering applied to it), a model of the form:

$$m(t) = a_0 + \sum_{i=1}^{10} (a_i \cos(2\pi i t/P) + b_i \sin(2\pi i t/P))$$

$$+ \sum_{i=1}^N c_i s_i(t). \quad (6)$$

The first sum is a Fourier series with period P (the period found for the light curve in section 3) which is used to represent the physical signal, while the second sum is a model for the instrumental/atmospheric variations. The free parameters in this model are the a_i , b_i and c_i coefficients, while the $s_i(t)$ terms, which represent instrumental variations, consist of 530 template light curves, together with 14 known instrumental parameter sequences (including: the X and Y subpixel positions of the star to first and second order, 3 parameters describing the PSF shape to first and second order, the hour angle, the zenith angle, the background, and the deviation of the background). Because all free parameters enter linearly in eq. 6, the fit can be done quickly using singular value decomposition (e.g. Press et al. 1992).

We take the amplitude of the light curve to be equal to the peak-to-peak amplitude of the Fourier series in eq. 6. For four stars, HAT-259-0000690 (PELS 020), HAT-259-0000923 (HII 120), HAT-260-0000924 (HII 1182) and HAT-260-0007928 (HII 906), with periods very close to 3, 4, 3 and 2 days respectively, the poor phase coverage of the HAT-Net light curves means that the high order harmonics in the Fourier series are not well constrained. For these stars we therefore do not include any harmonics other than the fundamental (i.e. the Fourier series includes one term only) when fitting equation 6.

The median value of the ratio of amplitudes from signal *reconstruction* EPD/TFA light curves to amplitudes from signal *recovery* EPD/TFA light curves is 1.3. This illustrates the importance of using signal reconstruction EPD/TFA to get an unbiased amplitude measurement.

3.4 Catalogue of Rotation Periods for Pleiades Members

Using the recent compilation of probable Pleiades members by Stauffer et al. (2007, hereafter S07), we identify 470 probable members with magnitudes in the range $9.5 < r < 14.5$ for which we have obtained light curves. We detect periodic variations for 350 of these stars (i.e. 74% of them); for stars with $11 < r < 13$, our period detection rate is 93%. Faint stars with $13 < r < 14.5$ have low photometric precision making it more difficult to detect their variations, while hotter stars with $9.5 < r < 11$ have lower amplitudes of variation. Stars with $9.5 < r < 10$ may also be saturated in a significant fraction of the images. As a comparison, for stars with $11 < r < 13$ that are not selected as probable cluster members, the period detection rate is 9.8%. Two factors that lead to a much higher incidence of variability for Pleiades stars include their young age relative to field stars (so that they are more active and have higher amplitudes of variability), and the fact that the majority of field stars are more distant than the Pleiades, so Pleiades stars of a given mass are brighter, and have higher precision light curves, than most field stars of that mass in the survey.

Our final catalogue of rotation periods is included in the supplementary material to the online edition of this article. Table 1 shows a portion of the catalogue for guidance regarding its form and content. We include in the catalogue

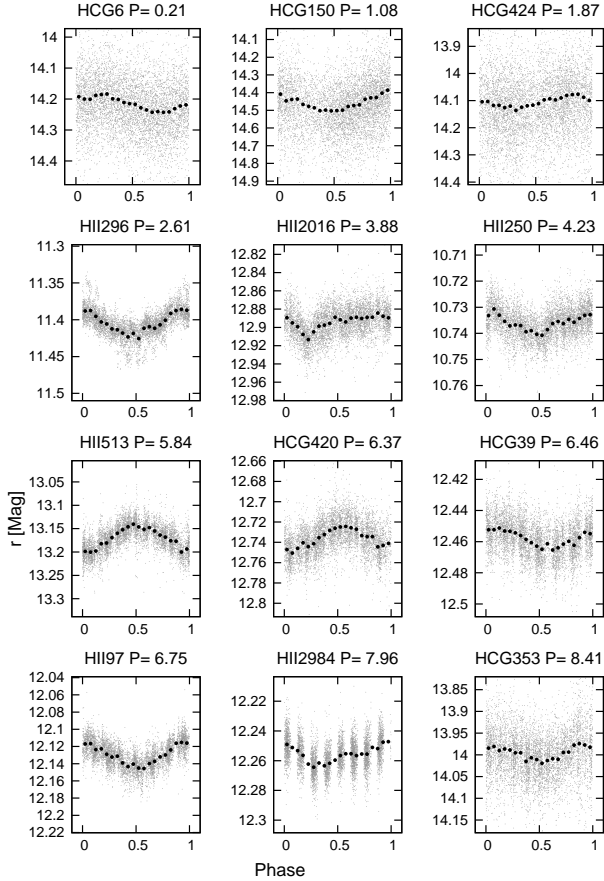


Figure 5. Phased light curves for 12 stars randomly selected from our catalogue, sorted by rotation period. The gray-scale points show all the photometric data, the dark filled circles show the phase-binned light curve. The name for each star is taken from Stauffer et al. (2007) and the listed period is in days. These light curves have had signal-reconstruction EPD/TFA applied (Section 3.3).

fifteen stars with rotation periods in the literature that we do not recover, including the star CFHT-PL 8 which was not included in the S07 catalogue, and exclude one star with a period in the literature that is not a cluster member (see Section 4.1 for further details on these stars). We also include 18 variable stars which are not in the S07 catalogue, but which have photometry, proper motions, and periods consistent with cluster membership (see section 3.5 below).

Figure 5 shows phased light curves for 12 stars randomly selected from our catalogue, while figure 6 shows L-S periodograms for 3 of these stars. Figure 6 also shows an example of a star which is not selected after applying the red-noise correction to the periodogram (equation 3). The photometric light curves for all 488 probable members observed with HATNet will be made publicly available from the NASA Star and Exoplanet Database (NStED; von Braun et al. 2009)¹.

In addition to the catalogue of rotation periods, we also provide a catalogue of Pleiades stars observed with HATNet

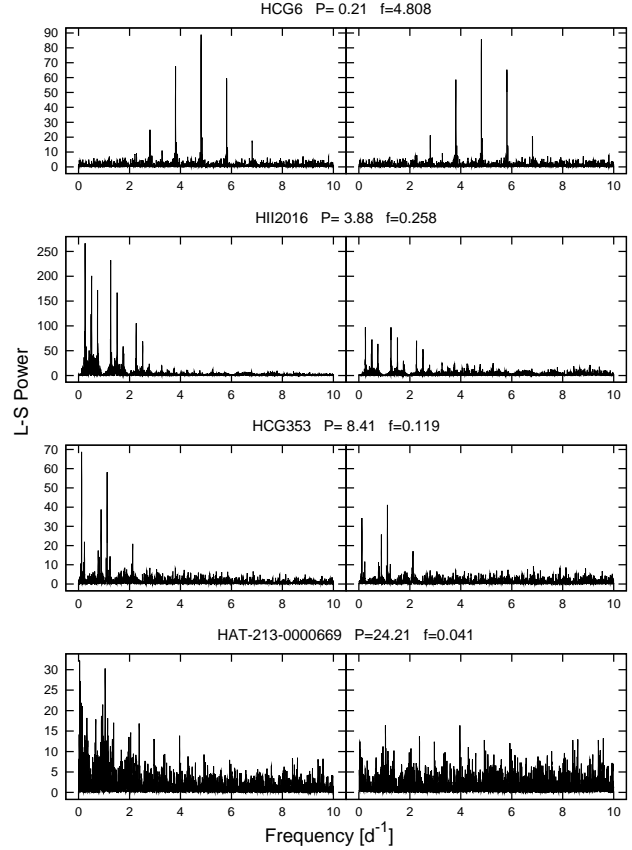


Figure 6. L-S periodograms for 3 of the stars displayed in figure 5, and for a fourth field star which passes the S/N selection before applying the red-noise correction to the periodogram (equation 3), but does not pass the selection after applying the correction. For each star we show the original L-S periodogram on the left, and the red-noise corrected periodogram on the right. We list the period (in days) and the frequency (in cycles per day) selected for each star. For the star in the bottom panel, this is the period that is selected from the un-corrected periodogram. For HCG 353 the low frequency alias is adopted following the procedure described in Section 3.1.

for which we do not detect a period (Table 2), a catalogue of field variable stars (Table 3), and a list of previous period measurements for Pleiades stars (Table 4).

3.5 New Cluster Members

Here we leverage the enhanced photometric variability of Pleiades stars relative to field stars to identify new members of the cluster. A similar method for selecting Pleiades members was employed by Haro et al. (1982) who identified flare stars as candidate members. More recently, Collier Cameron et al. (2009) used photometric variability to select members of the Coma Berenices open cluster.

Figure 7 shows the selection of cluster members. We first select variable stars that are within 5° of the centre of the cluster, and are near the cluster main sequence on a $J - K_S$ colour-magnitude diagram (CMD), taking the photometry from the 2MASS $6 \times$ PSC (see the description by Cutri et

¹ <http://nsted.ipac.caltech.edu>

al.²) when available, and from the main 2MASS PSC for all other stars. A total of 221 of the 958 variables not included in the S07 catalogue that are within 5° of the cluster centre pass this selection. Of these, 189 have proper motions from the PPM-Extended catalogue (Röser et al. 2008), while 28 of the remaining 32 stars have proper motions from the USNO-B1.0 catalogue (Monet et al. 2003). To establish the proper motion membership probability we follow the procedure outlined in Deacon & Hambly (2004). Briefly, we assume that proper motions are distributed as:

$$\Phi = f\Phi_f + (1 - f)\Phi_c \quad (7)$$

where f is the fraction of stars in the field, Φ_f is the distribution for field stars, and Φ_c is the distribution for cluster members. We assume bivariate Cauchy distributions for the field and the cluster of the form:

$$\Phi_f = \frac{1}{2\pi\Gamma_f^2} \frac{1}{1 + ((\mu_x - \mu_{xf})^2 + (\mu_y - \mu_{yf})^2)/\Gamma_f^2)} \quad (8)$$

$$\Phi_c = \frac{1}{2\pi\Gamma_c^2} \frac{1}{1 + ((\mu_x - \mu_{xc})^2 + (\mu_y - \mu_{yc})^2)/\Gamma_c^2)} \quad (9)$$

where μ_x and μ_y are the proper motion in the right ascension and declination directions respectively. We determine the free parameters f , μ_{xf} , μ_{yf} , μ_{xc} , μ_{yc} , Γ_f and Γ_c by using the downhill simplex algorithm to maximize the likelihood function

$$L = \sum_i \ln \Phi_i \quad (10)$$

where the sum is over all variable stars. We also attempted to use Gaussian and Exponential distributions for Φ_f and Φ_c , but found that the Cauchy distributions provided the best match to the observations. The membership probability for a star is then given by

$$p = \frac{(1 - f)\Phi_c}{f\Phi_f + (1 - f)\Phi_c}. \quad (11)$$

We require $p > 70\%$ for the star to be considered a probable member. Of the 22 stars which pass the above selections, we reject 4 with periods longer than any known cluster members of comparable magnitude.

Four of the 18 remaining probable cluster members have previously been selected as potential cluster members, but were not included in the S07 catalogue. These include HCG 84 and HCG 235, two well-known flare stars included in the catalogue of Pleiades members by Haro et al. (1982), and in several subsequent membership catalogues, and the stars SRS 79807 and SRS 34337 which were identified as proper-motion members by Schilbach et al. (1995), but to our knowledge, have not appeared in subsequent studies. All 18 stars are included in the rotation period catalogue.

4 DISCUSSION

4.1 Comparison With Other Period Measurements

To compare our measurements to previous observations of the Pleiades, we use the compilation of rotation periods

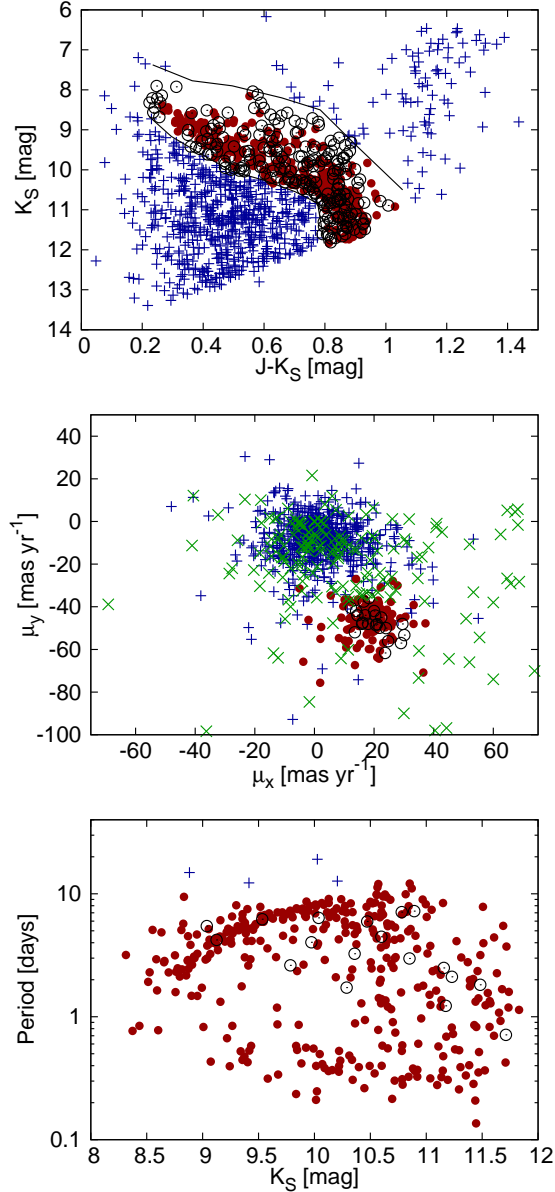


Figure 7. Top: $J - K_S$ CMD for all variable stars. Cluster members from S07 are plotted with filled circles, variables with $J - K_S$ photometry consistent with cluster membership are plotted with open circles, and variables that are not photometric members are plotted with crosses. The solid lines delineate the selection of candidate cluster members. Centre: Vector Point Diagram (VPD) for all identified variable stars. Filled circles show cluster members from S07, crosses are stars which were rejected as non-photometric members in the left panel, open circles show photometric members which also have a proper motion membership probability $> 70\%$, Xs show photometric members which have a proper motion membership probability $< 70\%$. Bottom: Period vs. K_S -magnitude. Filled circles show cluster members from S07, open circles correspond to new candidate members which passed the other two selections and also have periods that are consistent with cluster membership. Crosses show candidate members that passed the previous selections, but have periods that are too long to be cluster members.

² <http://www.ipac.caltech.edu/2mass/releases/allsky/doc/seca3.1.html>

provided on the WEBDA database³. The original measurements come from a variety of sources (Stauffer et al. 1987; Prosser et al. 1993a,b, 1995; Marilli, Catalano & Frasca 1997; Krishnamurthi et al. 1998; Terndrup et al. 1999; Messina 2001; Clarke, MacDonald, & Owens 2004; Scholz & Eislöffel 2004). We also include periods for 11 stars from van Leeuwen, Alphenaar, & Meys (1987) that are not listed on WEBDA. A total of 66 stars are included in the compilation, which is provided in table 4.

We recover rotation periods for 50 of the stars with previous measurements. Here we discuss the 16 stars with previous measurements which we do not recover. The 9 very low-mass stars studied by Scholz & Eislöffel (2004) are all too faint to be observed with HATNet, the star HD 23386 studied by Marilli, Catalano & Frasca (1997) and Messina (2001) is saturated in our images. There are four stars that we observed but did not detect a period for, including: HII 708 (Prosser et al. 1993b; Marilli, Catalano & Frasca 1997), HII 727 (Prosser et al. 1993b; Marilli, Catalano & Frasca 1997), HII 975 (Marilli, Catalano & Frasca 1997) and HHJ 409 (Terndrup et al. 1999). The first three of these stars are near the bright end of the magnitude range covered by HATNet, while HHJ 409 is near the faint end. Finally there are two stars listed as variables on WEBDA that are not included in the S07 catalogue. One of these stars, HII 3167, was reported to be variable by Clarke, MacDonald, & Owens (2004) with a 0.25 mag amplitude in *B*, 0.15 mag amplitude in *V* and a period of ~ 0.9 d. We find no evidence for variability in our light curve for this star (we match the star to 2MASS J2000.0351555+2442326 based on the plate *x/y* position given on WEBDA, however this identification may not correspond to the same star observed by Clarke, MacDonald, & Owens 2004). In any case the star is not a cluster member (based on the color and magnitude given by Clarke, MacDonald, & Owens 2004), so we do not include it in the final catalogue of Pleiades variables. The other known variable that is not in the S07 catalogue is CFHT-PL 8 (Bouvier et al. 1998), which was identified as a variable by Terndrup et al. (1999). This very low mass star is too faint to be observed by HATNet. We include it in the final catalogue of rotation periods, with coordinates and K_S photometry taken from the 2MASS catalogue, and *V* magnitude taken from Samus et al. (2003).

For 44 of the 50 previously studied stars that we recover, our frequency is within 0.1 d^{-1} of at least one of the previously published frequencies for the star; and for 35 stars our frequency is within 0.01 d^{-1} of at least one of the previously published frequencies. Figure 8 shows a comparison of the rotation frequencies measured in our survey to those given in the literature for stars with previous measurements. Below we discuss the 6 cases where our frequencies are substantially different from all of the literature values:

HII 250 - Has published periods of 0.843 days from Marilli, Catalano & Frasca (1997) and 0.591 days from Messina (2001). We measure a period of ~ 4.232 days. Our light curve shows no evidence for periodicity at either of the published periods.

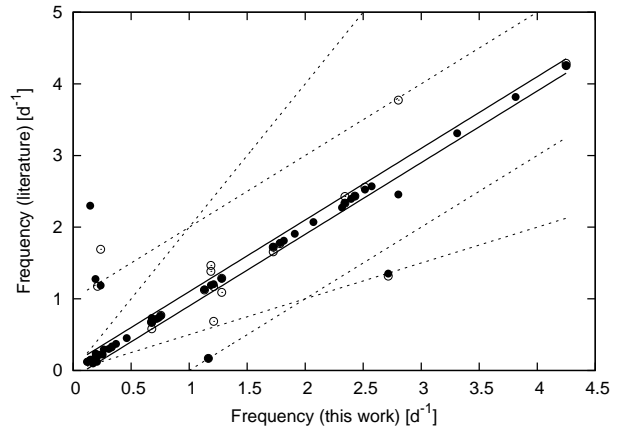


Figure 8. Comparison between the rotation frequencies measured in our survey and those given in the literature for stars with previous measurements. For stars with multiple frequencies given in the literature, we show the literature value that is closest to our own (filled circles); the open circles show the other literature values for these stars. Points between the solid lines have literature frequencies that are within 10% of our frequencies. The dotted lines show the $\pm 1 \text{ d}^{-1}$ alias frequencies, and the 2.0 and 0.5 harmonic frequencies.

HII 335 - Has published periods of 0.265 days from Stauffer et al. (1987) and 0.4073 days from Messina (2001). Stauffer et al. (1987) also report an alias period of 0.360 days for this star that is consistent with our measured period of 0.357 days.

HII 885 - The only published period for this star is 0.435 days from Marilli, Catalano & Frasca (1997). We measure a period of 6.83 days, and find no evidence for periodicity at 0.435 days.

HII 1039 - The only published period for this star is 0.784 days from Messina (2001). We measure a period of 5.22 days, and find no evidence for periodicity at 0.784 days.

HII 1124 - Has published periods of 5.9 days from Prosser et al. (1995) and 6 days from van Leeuwen, Alphenaar, & Meys (1987). We find a period of 0.858 days for this star, however prior to correcting the periodogram for red-noise the top peak in the periodogram for this star is at 6.133 days. This star has $v \sin i = 3.50 \text{ km s}^{-1}$ (Queloz et al. 1998), which is closer to the expected equatorial rotation velocity of $\sim 5.8 \text{ km s}^{-1}$ for the ~ 6 day period than the velocity of $\sim 40 \text{ km s}^{-1}$ for the shorter period. We therefore adopt the longer period for the final catalogue.

HII 1653 - Both Krishnamurthi et al. (1998) and Messina (2001) measured periods of ~ 0.75 days for this star. Our period of 0.368 days is half the value of the published periods, and is inconsistent with the previously published light curves for the star. We therefore double our period for the final catalogue.

4.2 Comparison with $v \sin i$ data

We compare our period measurements to the rich sample of $v \sin i$ measurements available for members of the Pleiades. Measurements of $v \sin i$ are taken from Stauffer et al. (1987), Soderblom et al. (1993), Queloz et al. (1998), and

³ <http://www.univie.ac.at/webda/webda.html>

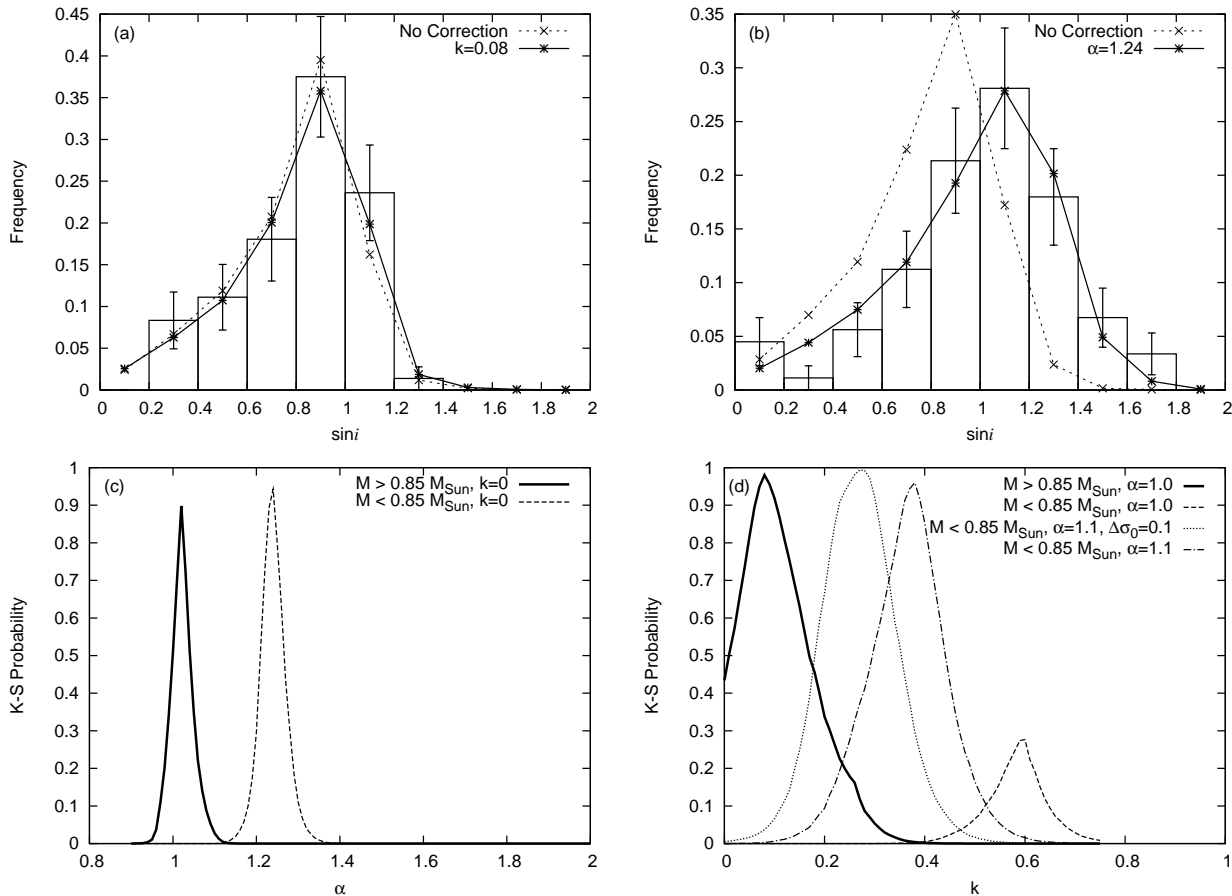


Figure 10. The distribution of $\sin i$ values for stars with $M > 0.85 M_{\odot}$ (a) and for stars with $M < 0.85 M_{\odot}$ (b). These are compared to the expected distribution assuming stars have random rotation axis orientations and that there are no systematic biases in the measured parameters (the “No Correction” line), as well as to a model that includes differential rotation (the $k = 0.08$ line in panel (a)), and a model that includes a scale factor α applied to the $\sin i$ values (the $\alpha = 1.24$ line in panel (b)). We also show the probability that the observed $\sin i$ distribution is drawn from a model distribution for models invoking a scale factor α (c) and for models that include differential rotation (d).

Terndrup et al. (2000). A total of 223 of the stars for which we detect periods also have a $v \sin i$ value given in one of these sources.

Figure 9 compares the photometric rotation periods and the $v \sin i$ values, and also compares the inferred $\sin i$ to the stellar mass. The results are shown separately for objects selected as lying on the single-star main sequence, and objects selected as photometric binaries (see figure 13). For the remainder of this analysis we only consider nonphotometric binaries. The value for $\sin i$ is determined from:

$$\sin i = \frac{v \sin i \cdot P}{2\pi R} \quad (12)$$

where $v \sin i$ is the measured value of the projected equatorial rotation velocity, P is the measured rotation period, and R is the stellar radius. We estimate the stellar radius from the M_K magnitude using the 125 Myr, solar metallicity (the Pleiades have $[\text{Fe}/\text{H}] = +0.03 \pm 0.05$; Soderblom et al. 2009), Yonsei-Yale isochrone (Y2; Yi et al. 2001). We transform the isochrone to the 2MASS system from the ESO system using the transformations given by Carpenter (2001). To determine the absolute magnitudes we assume a distance to the Pleiades of 133 pc (Soderblom et al. 2005) and

an extinction of $A_K = 0.01$ mag (S07). Note that if we instead adopt a distance of 120.2 pc to the cluster based on Hipparcos parallax measurements (van Leeuwen 2009), and assume the same extinction and M_K -mass and M_K -radius relations, the inferred stellar masses and radii at fixed K_S magnitude are lower by $\sim 10\%$. Also note that if we use the Baraffe et al. (1998) isochrone models for stars with $M \sim 0.4 M_{\odot}$, the inferred masses at fixed K_S are lower by $\sim 8\%$, while the inferred radii are lower by $\sim 30\%$. The inferred radius also depends on the assumed age for the cluster. The assumed age of 125 Myr for the Pleiades from Stauffer et al. (1998) is based on the observed Li-depletion of main sequence stars in the cluster, a method which has recently been called into question for other stellar populations (Jeffries et al. 2009; Yee & Jensen 2010). Determinations of the age of the Pleiades from the main sequence turn-off range from ~ 80 Myr (Mermilliod 1981) to ~ 150 Myr (Mazzei & Piggato 1989). Adopting a younger age of 80 Myr for the cluster will increase the radii of stars at fixed $mass$; the affect on the M_K -radius relation, however, is less significant, as stars with fixed mass will also be brighter in M_K at younger ages. By comparing the M_K -radius relation obtained from the 80 Myr solar-metallicity isochrone from

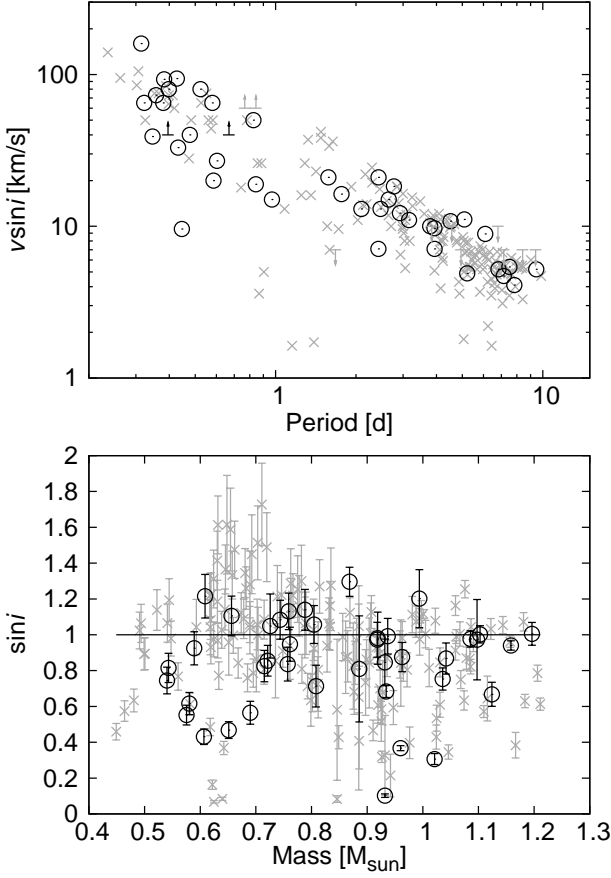


Figure 9. Top: The spectroscopically determined $v \sin i$ taken from the literature vs. the photometric rotation period determined in this paper for 223 stars. Open circles show objects selected as photometric binaries and grey-scale Xs show non-binaries. Arrows show stars for which only upper or lower limits on $v \sin i$ are available. Bottom: $\sin i$ calculated from $v \sin i$, the rotation period, and the radii inferred from an isochrone (see section 4.2 for details). Stars falling above the line $\sin i = 1$ have measured rotation period, $v \sin i$ and stellar radius values that are not fully consistent with one another. The error-bars include uncertainties in $v \sin i$, the period, and the radius (propagated from the uncertainty on K_s). We assume a 10% uncertainty on $v \sin i$ for stars without $v \sin i$ uncertainties given in the literature. We exclude known and suspected spectroscopic binary systems from both plots.

Siess et al. (2000) using the Kenyon & Hartmann (1995) temperature-colour relations, to the 125 Myr isochrone from the same models⁴, we estimate that the systematic error in the radius that may result from overestimating the age of the cluster is $\lesssim 2\%$ over the magnitude range of interest. Finally if we use the M_V magnitude to determine the radii from the Y2 isochrones, rather than the M_K magnitude, the inferred radii for most stars are lower by up to $\sim 25\%$.

As seen in Figure 9, the $\sin i$ values determined with

⁴ We use the Siess et al. (2000) isochrones rather than the Y2 isochrones because the Y2 isochrones do not cover the pre-main sequence stage of stellar evolution.

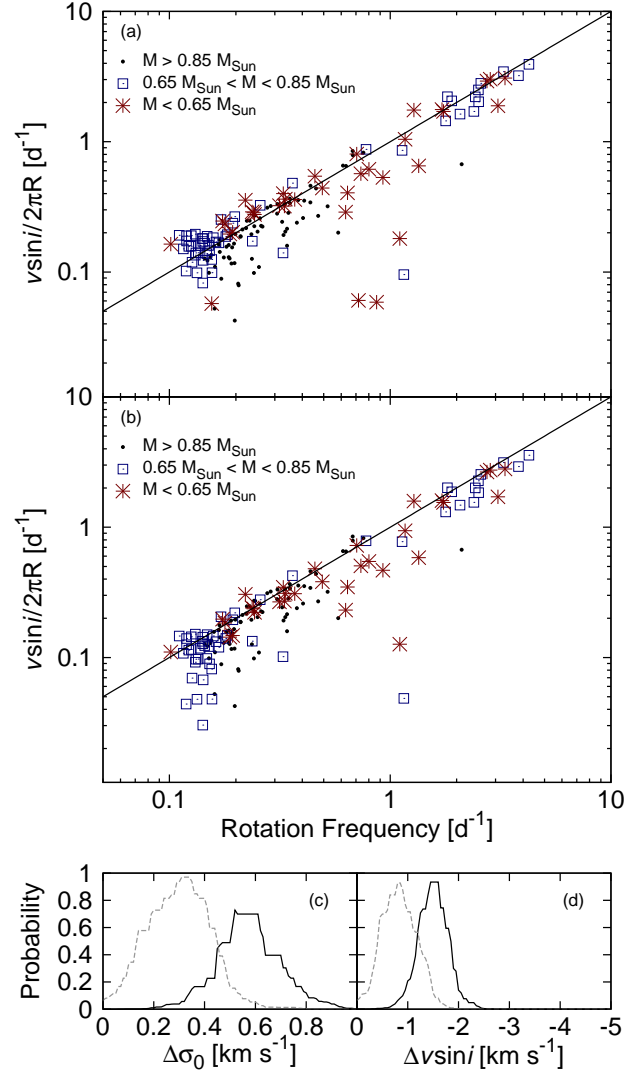


Figure 11. a: Photometric rotation frequency ($1/P$) vs. the frequency inferred from $v \sin i$. The solid diagonal line shows the upper limit ($\sin i = 1$). The stars are divided into three mass bins. Low frequency (long period) stars with $M < 0.85 M_\odot$ are more likely to lie above the upper limit than higher frequency stars with comparable masses. Stars with $M > 0.85 M_\odot$ generally fall below the upper limit for all frequencies. b: Same as above, here the velocities of stars with $M < 0.85 M_\odot$ have been corrected with $\Delta\sigma_0 = 0.16 \text{ km s}^{-1}$, and the radii of these stars have been increased by 10%, see the text for details. c: The probability that stars with $M < 0.85 M_\odot$ have the same $\sin i$ distribution as stars with $M > 0.85 M_\odot$ as a function of the applied $\Delta\sigma_0$ correction. The solid line is for the case when no radius correction is applied, the dashed line shows the case when a 10% correction is applied to the radii of stars with $M < 0.85 M_\odot$. d: Same as C, here a $\Delta v \sin i$ correction is applied.

equation 12 are greater than 1 for many stars with $M \lesssim 0.85 M_\odot$. In Figure 10 we compare the observed distribution of $\sin i$ values to various model distributions. To calculate the model distributions we generate a sample of $\sin i$ values assuming the rotation axes of the stars are randomly oriented in space ($\cos i$ is uniformly distributed). We then as-

sign to each sample $\sin i$ value a gaussian error $\Delta \sin i$ taken from the set of errors associated with the actual data, and use these to generate a simulated sample of measured $\sin i_m$ values with the condition $\sin i_m > 0$. As discussed in section 3.2 differential rotation may cause the measured rotation periods to be systematically longer than the equatorial rotation periods. This effect will in turn cause the measured $\sin i_m$ values to be systematically greater than the true values. To include this effect in our models we associate with each simulated $\sin i$ value a latitude β for the dominant spot group. We assume that these spots may be uniformly distributed over the surfaces of the stars for reasons outlined in section 3.2, so we draw the values of β from a uniform distribution in $\sin \beta$. We then scale each $\sin i_m$ value by the factor $1/(1 - k \sin^2 \beta)$ (equation 5). Finally we parameterize any remaining systematic errors in the measured values of $\sin i$ by multiplying the $\sin i_m$ values by a constant scale factor α . We compare the models to the observations using the Kolmogorov-Smirnov test, recording the probability that the observed sample is drawn from the same distribution as the simulated sample as a function of the parameters k and α (figure 10 panels (c) and (d)).

For stars with $M > 0.85 M_\odot$, we find that the $k = 0$, $\alpha = 1$ distribution is consistent with the observed distribution (the K-S probability that the observed and model data-sets are drawn from the same distribution is $\sim 50\%$), while a $k = 0.08$, $\alpha = 1$ model (i.e. a model with differential rotation that is comparable to what is expected for young rapidly rotating stars) provides a slightly better match (90% probability). A similar result has recently been found in an independent study of the Pleiades and Alpha Persei by Jackson & Jeffries (2010) who placed limits on the degree to which the rotation axes of stars in these clusters are aligned.

For stars with $M < 0.85 M_\odot$ the probability that the $k = 0$, $\alpha = 1$ model is drawn from the same distribution as the observations is only $\sim 10^{-13}$. In this case a significant value of $\alpha = 1.24 \pm 0.05$ is required to fit the observations. If we fix $\alpha = 1.0$ and allow k to vary, the best matching model has a very high value of $k = 0.60$, with a probability of being drawn from the same distribution as the observations of less than 30%.

While the distribution of $\sin i$ values for $M > 0.85 M_\odot$ stars are consistent with the stars having random orientations and perhaps having a slight degree of differential rotation, the measured values of $\sin i$ for stars with $M < 0.85 M_\odot$ appear to be systematically too large (the mode is at $\sin i > 1$). The combination of measured parameters $Pv \sin i/R$ may be systematically larger by a factor of ~ 1.24 than the same combination using the real physical parameters would be. This suggests systematic errors in one or more of the parameters. Below we consider each of the parameters in turn.

Radius – While it is well-known that the radii of rapidly rotating stars with $M \lesssim 0.85$ are systematically larger than theoretical models predict (e.g. Fernandez et al. 2009, and references therein), the discrepancy appears to be $\sim 10\%$ and not 24%. If we adopt the Hipparcos distance of 120.2 pc to the cluster, use the Baraffe et al. (1998) isochrones rather than the Y2 isochrones, or use the V magnitude rather than the K magnitude to determine the radii, the inferred radii of the stars would be even smaller, exacerbating the $\sin i$ problem.

Period – While an extreme differential rotation law of $k = 0.60$ could fit the distribution, the match is still not very good. Alternatively if the dominant spot groups on lower mass Pleiades stars are not randomly distributed, but are instead preferentially located at high latitudes, this would cause the measured $\sin i$ values to be systematically larger than they would be if the spots are randomly distributed.

$v \sin i$ – The $v \sin i$ measurements of cool Pleiades dwarfs could be systematically biased toward larger values. Figure 11a compares the rotation frequency determined from the photometric period to the rotation frequency inferred from $v \sin i$ (i.e. $v \sin i / 2\pi R$). For stars with $M < 0.85 M_\odot$, it appears that lower frequency (longer period) stars are more likely to have $\sin i > 1$ than higher frequency (shorter period) stars. An offset error in $v \sin i$ would yield this effect. Most of the longer period, low-mass stars with $\sin i > 1$ have $v \sin i$ measurements taken from Queloz et al. (1998). These authors calculate $v \sin i$ from the broadening of a spectral cross-correlation function using the relation:

$$v \sin i = A \sqrt{\sigma^2 - \sigma_0^2} \quad (13)$$

where σ^2 is the measured width of the cross-correlation function and A and σ_0^2 are parameters which are calibrated by artificially broadening the observed spectra of slowly rotating field stars to a fixed value of $v \sin i$, and measuring the widths of the resulting cross-correlation functions. For the ELODIE spectrograph, Queloz et al. (1998) give $A = 1.9 \pm 0.1$, and

$$\sigma_0 = 0.27(B - V)^2 + 4.51(\pm 0.06) \quad (14)$$

where $B - V$ is the measured color of a star, and σ_0 is measured in km s^{-1} . A systematic error in σ_0 would impact slower rotators more significantly than faster rotators. To estimate the required systematic error in σ_0 , we adjust the velocities of stars with $M < 0.85 M_\odot$ by

$$\Delta v \sin i = - \frac{A^2 \sigma_0 \Delta \sigma_0}{v \sin i} \quad (15)$$

and use the K-S test to compare the resulting $\sin i$ distribution to the $\sin i$ distribution for stars with $M > 0.85 M_\odot$. For this test we assume $\sigma_0 = 4.8$ for these stars. Figure 11c shows the probability that the two samples are drawn from the same distribution as a function of $\Delta \sigma_0$. We conducted a similar test assuming a constant $\Delta v \sin i$ (figure 11d). We find $\Delta \sigma_0 = 0.6 \pm 0.2 \text{ km s}^{-1}$ or $\Delta v \sin i = -1.5 \pm 0.5 \text{ km s}^{-1}$ yields a $\sin i$ distribution for stars with $M < 0.85 M_\odot$ that is statistically indistinguishable from the distribution for stars with $M > 0.85 M_\odot$. If the isochrone radii of stars with $M < 0.85 M_\odot$ are also assumed to be 10% too low, we find $\Delta \sigma_0 = 0.33_{-0.27}^{+0.19} \text{ km s}^{-1}$ or $\Delta v \sin i = -0.85 \pm 0.63$. Figure 11b shows how a correction of $\Delta \sigma_0 = 0.33$, together with a 10% radius correction affects the frequencies inferred from $v \sin i$ for stars with $M < 0.85 M_\odot$. A systematic error of $\Delta \sigma_0 = 0.33_{-0.27}^{+0.19} \text{ km s}^{-1}$ is consistent at the 1σ level with the systematic uncertainty in σ_0 of $\sim 0.06 \text{ km s}^{-1}$ estimated by Queloz et al. (1998). Differences between the young Pleiades stars and the older field stars used to calibrate the $(B - V) - \sigma_0$ relation could result in an even greater systematic error in σ_0 . For example, Stauffer et al. (2003) showed that Pleiades stars do not have typical spectral energy distributions—in particular they have excess emission in the B band (and are therefore *bluer* in $B - V$ than expected from their effective temperatures). Equation 14 may therefore underes-

timate the intrinsic broadening of Pleiades K dwarfs. Quantitatively, a 0.1 mag shift in $B - V$ for Pleiades stars with $B - V \sim 1.0$ yields an additional $\sim 0.05 \text{ km s}^{-1}$ shift in σ_0 .

In conclusion, assuming that the radii are systematically underestimated by $\sim 10\%$, and that the intrinsic broadening of these stars are also underestimated by $\sim 0.1 \text{ km s}^{-1}$, we find that the observed distribution of $\sin i$ values would then be consistent with the model distribution for a differential rotation parameter of $k = 0.27 \pm 0.14$ (the $M < 0.85 M_\odot$, $\alpha = 1.1$, $\Delta\sigma_0 = 0.1$ line in figure 10d). Allowing for a larger error in the intrinsic broadening would reduce the required k . If we only apply the radius correction, the differential rotation parameter would need to be rather large ($k = 0.38^{+0.12}_{-0.15}$; the $M < 0.85 M_\odot$, $\alpha = 1.1$ line in figure 10d). We conclude that some combination of the above effects provides a plausible explanation for the large number of low-mass stars with measured $\sin i > 1$.

Finally, we note that a qualitatively similar effect has also been noted by Jackson et al. (2009) for stars with $0.2 M_\odot < M < 0.7 M_\odot$ in the comparably aged open cluster NGC 2516. They find that the radii of stars with $M \sim 0.2 M_\odot$ must be $\sim 50\%$ larger than theoretical predictions for the $v \sin i$ and period data to be consistent in this cluster.

4.3 The Period-Mass Relation and Comparison to Other Clusters

Figure 12 shows the rotation period vs. absolute magnitude M_K and mass, together with the relation between $v \sin i$ and absolute magnitude M_K /mass. By comparing the $v \sin i$ values of stars without photometric period detections to the $v \sin i$ values of stars with period detections, it is apparent that over the mass range $0.6 M_\odot \lesssim M \lesssim 1.0 M_\odot$ there does not appear to be a bias against detecting photometric periods for slow rotators. For star with $M \gtrsim 1.0 M_\odot$ there does appear to be a bias against detecting periods for the slowest rotators, so our sample is not complete in this mass range. For stars with $M \lesssim 0.6 M_\odot$ the bias appears to be against detecting rapid rotators. This is likely due to short period stars being redder on average than long period stars (see Fig. 13 which demonstrates this for $(V - K_S)$, this is likely to be true for $(r - K_S)$ as well), so that at fixed K_S short period stars are fainter in r than long period stars, and therefore have poorer precision HATNet light curves.

In figure 14 we compare the period-mass relation for the Pleiades to the relations for four other similarly aged clusters. These include 3 clusters studied by the MONITOR project (NGC 2547, 40 Myr, Irwin et al. 2008; M50, 130 Myr, Irwin et al. 2009; and NGC 2516, 150 Myr, Irwin et al. 2007), and the cluster M35 (180 Myr, Meibom et al. 2009). For the MONITOR clusters we adopt the stellar masses given in their tables. For M35 we determine stellar masses using the extinction corrected V -magnitudes given by Meibom et al. (2009) together with the Y2 isochrones. We assume an age of 180 Myr (Kalirai et al. 2003), distance of 912 pc (Kalirai et al. 2003), and metallicity of $[\text{Fe}/\text{H}] = -0.21$ (Schuler et al. 2003).

The data presented here can be combined with data for other open clusters to test theories of stellar angular momentum evolution. While a sophisticated analysis like that presented by Denissenkov et al. (2009) is beyond the

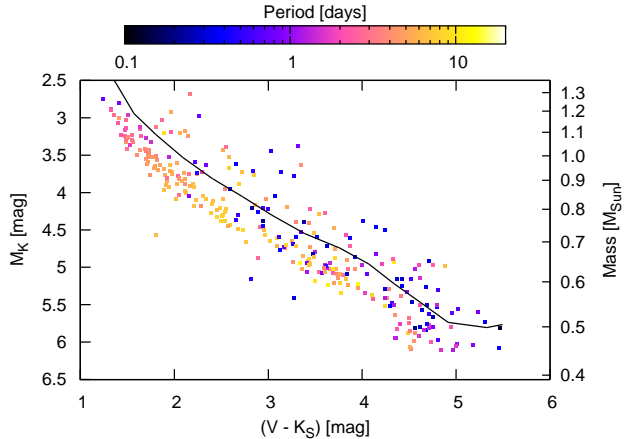


Figure 13. $(V - K_S)$ vs. M_K CMD for probable Pleiades members with detected rotation periods. The color-intensity of each point is scaled by the star’s rotation period. At fixed M_K , short period rotators tend to be redder in $(V - K_S)$ than long period rotators. This effect was previously noticed using $v \sin i$ data by Stauffer et al. (2003) for Pleiades stars and by An et al. (2007) for stars in NGC 2516. Stauffer et al. (2003) suggested that this effect may be due to rapid rotators having more red spots than slow rotators. Alternatively this may be due to strong magnetic fields in rapid rotators inhibiting convection, which causes these stars to be larger and cooler than slow rotators (e.g. Chabrier et al. 2007). Stars located above the solid line are selected as potential photometric binaries, and are excluded from the analysis in section 4.2.

scope of this paper, it is instructive to compare the Pleiades sample to M35. As seen in figure 15, the main period-mass sequences in the two clusters overlap, indicating that slow rotators with $0.7 M_\odot \lesssim M \lesssim 1.1 M_\odot$ do not spin-down between 125 Myr and 180 Myr. We also show in figure 15 the substantial expected evolution between the two clusters for a standard solid-body rotation angular-momentum evolution model (e.g. Hartman et al. 2009a). While the slowly rotating stars do not spin-down between the ages spanned by the two clusters, more rapid rotators with $M \gtrsim 0.7 M_\odot$ do appear to have spun-down. These two features can be reproduced by models that invoke core-envelope decoupling with a coupling time-scale that depends on the rotation period, such that rapid rotators have a short coupling time-scale of a few Myr, while slow rotators have a long time-scale of ~ 100 Myr (Bouvier 2008; Denissenkov et al. 2009). As noted by Bouvier (2008), one consequence of slow rotators having a less efficient core-envelope coupling than rapid rotators is that slower rotators should exhibit more significant Li depletion than rapid rotators. Such an effect has been seen by Soderblom et al. (1993) for the Pleiades.

5 SUMMARY

In this paper we have presented new rotation period measurements for 368 stars in the Pleiades, increasing by a factor of 5 the number of stars in this cluster with measured periods. This includes 14 newly identified probable cluster members. The sample is $\sim 93\%$ complete for stars with $0.7 M_\odot \lesssim M \lesssim 1.0 M_\odot$. By comparing our sample to the

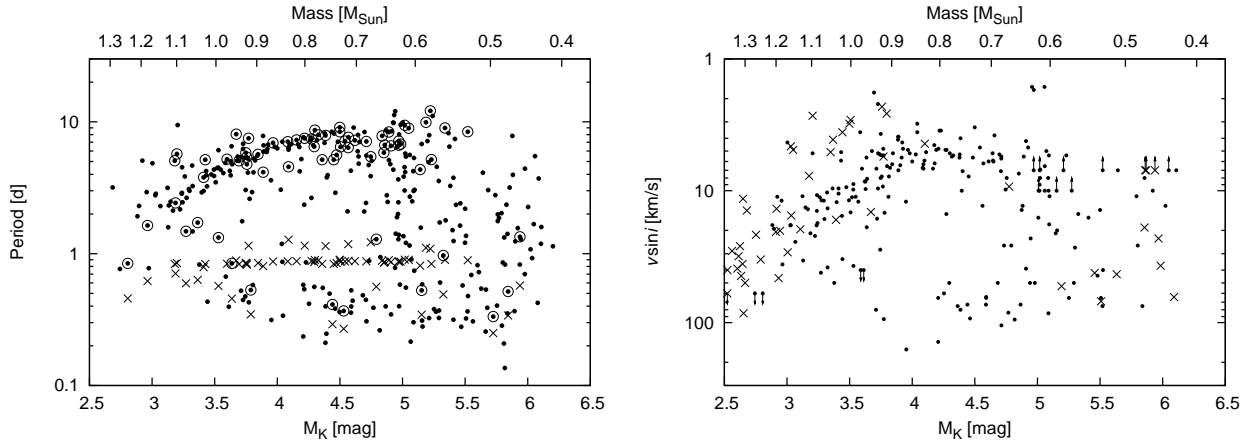


Figure 12. Left: photometric rotation period vs. the K_S absolute magnitude/mass for 350 probable members of the Pleiades cluster. Note that the period is plotted on a logarithmic scale. Filled circles show the adopted period values. Crosses show the periods prior to applying the alias correction described in section 3.1. Open circles show the periods after this correction. Right: spectroscopically measured $v \sin i$ vs. the K_S absolute magnitude/mass for stars in our sample with measured photometric rotation periods (filled circles) and stars without photometric rotation periods (crosses). Note that $v \sin i$ is plotted on an inverted logarithmic scale. For stars with $0.6 M_\odot \lesssim M \lesssim 1.0 M_\odot$ the sample with measured periods is nearly complete, and there does not appear to be any significant bias toward selecting fast rotators. For stars with $M \gtrsim 1.0 M_\odot$ there does appear to be a bias toward detecting photometric periods for faster rotators. For stars with $M \lesssim 0.6 M_\odot$ there may be a bias against selecting shorter period rotators. This is likely due to rapid rotators having slightly redder ($V - K_S$) colors at fixed K_S magnitude (fig. 13), making fast rotators slightly fainter in the r filter used by HATNet than slower rotators at fixed K_S .

large sample of Pleiades stars with $v \sin i$ measurements in the literature, we find that our sample is not biased toward short periods over this same mass range.

We show that for stars with $M \gtrsim 0.85 M_\odot$ the inferred distribution of $\sin i$ values is consistent with the stars having an isotropic distribution of rotation axes at the 1σ level, the agreement between the model and observations is even better if a $k = 0.08$ differential rotation law is assumed; a differential law of this form is consistent with theoretical expectations for zero-age main sequence stars. This result is consistent with the findings of Jackson & Jeffries (2010). For stars with $M \lesssim 0.85 M_\odot$ the inferred $\sin i$ values are systematically larger than 1, and is similar to what was seen by Jackson et al. (2009) for stars in NGC 2516. Our observations imply that the combination $P(v \sin i)/R$ is too large by $\sim 24\%$. We argue that a $\sim 10\%$ systematic error in the radii of these stars, together with a $\gtrsim 0.1 \text{ km s}^{-1}$ systematic error in the assumed intrinsic broadening of their spectral lines, and a $k \sim 0.3$ differential rotation law provides a plausible explanation for this discrepancy.

Finally, we find that the mass-period diagram for the Pleiades is remarkably similar to that seen by Meibom et al. (2009) for the ~ 185 Myr cluster M35. In particular there appears to be very little change in the rotation rates of the slowest rotators with $0.7 M_\odot \lesssim M \lesssim 1.1 M_\odot$ between the ages of these clusters. This result provides support for claims that these stars have inefficient internal angular momentum transport, and exhibit significant core-envelope decoupling.

ACKNOWLEDGMENTS

HATNet operations have been funded by NASA grants NNG04GN74G, NNX08AF23G and SAO IR&D grants. G.Á.B. acknowledges support from the Postdoctoral Fel-

lowship of the NSF Astronomy and Astrophysics Program (AST-0702843). G.K. thanks the Hungarian Scientific Research Foundation (OTKA) for support through grant K-81373. This research has made use of the SIMBAD database, operated at CDS, Strasbourg, France. This research has made use of the VizieR catalogue access tool, CDS, Strasbourg, France. This research has made use of the WEBDA database, operated at the Institute for Astronomy of the University of Vienna. This research has made use of the NASA/ IPAC Infrared Science Archive, which is operated by the Jet Propulsion Laboratory, California Institute of Technology, under contract with the National Aeronautics and Space Administration.

REFERENCES

- An, D., Terndrup, D. M., Pinsonneault, M. H., Paulson, D. B., Hanson, R. B., & Stauffer, J. R. 2007, *ApJ*, 655, 233
- Bakos, G., Noyes, R. W., Kovács, G., Staneik, K. Z., Sas-selov, D. D., & Domsa, I. 2004, *PASP*, 116, 266
- Bakos, G. Á., et al. 2010, *ApJ*, 710, 1724
- Baraffe, I., Chabrier, G., Allard, F., & Hauschildt, P. H. 1998, *A&A*, 337, 403
- Barnes, S. A. 2007, *ApJ*, 669, 1167
- Bilir, S., Ak, S., Karaali, S., Cabrera-Lavers, A., Chonis, T. S., & Gaskell, C. M. 2008, *MNRAS*, 384, 1178
- Bouvier, J., Stauffer, J. R., Martín, E. L., Barrado y Navascués, D., Wallace, B., & Béjar, V. J. S. 1998, *A&A*, 336, 490
- Bouvier, J. 2008, *A&A*, 489, L53
- Brown, B. P., Browning, M. K., Brun, A. S., & Toomre, J. 2004, in *Proc. SOHO 14/GONG 2004 Workshop* (ESA

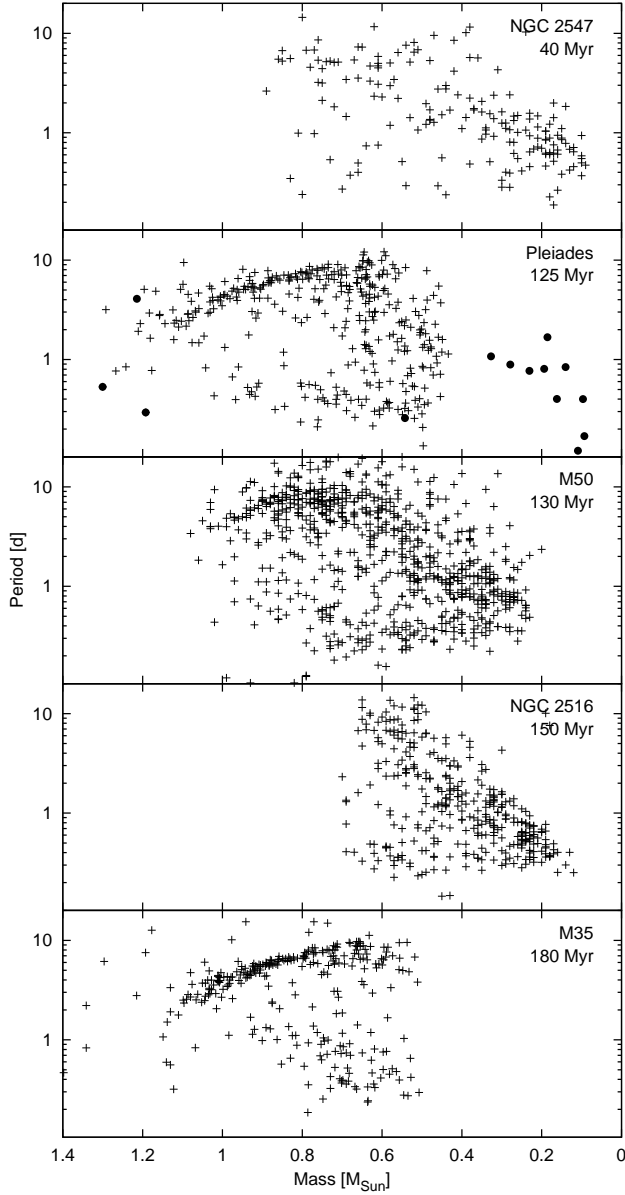


Figure 14. Comparison of the mass-period relation in the Pleiades to four other open clusters with similar ages. For the Pleiades diagram we include 14 stars from the literature which are either too faint to be included in the HATNet survey, or did not have periods recovered from the HATNet light curves (see section 4.1). These stars are marked with filled circles. The star HD 23386, which has an estimated mass of $\sim 1.47 M_{\odot}$, falls outside the plotted mass range.

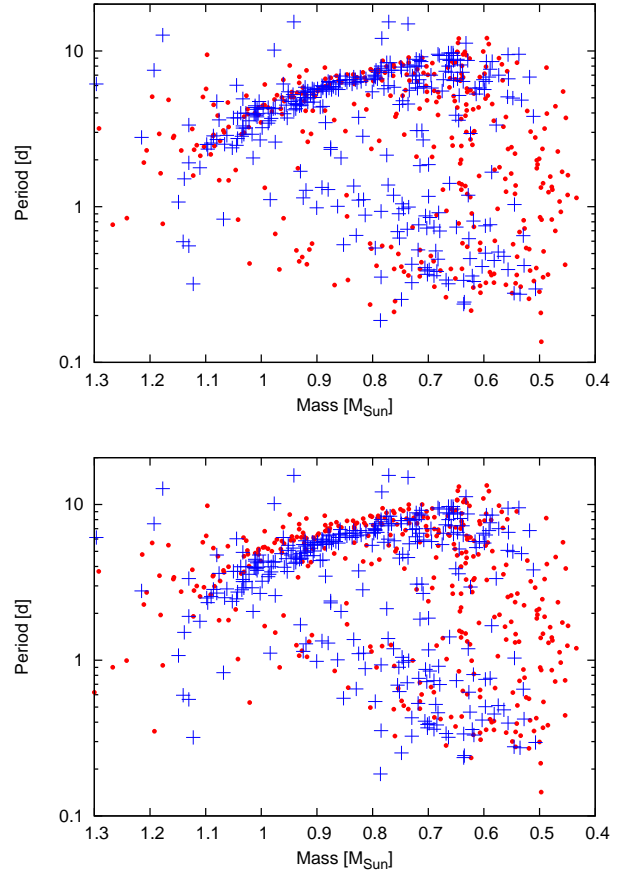


Figure 15. Top: Comparison of the mass-period relation in the Pleiades (filled circles) and M35 (crosses). Stars on the main mass-period sequence with $0.7 M_{\odot} \lesssim M \lesssim 1.1 M_{\odot}$ do not show significant period evolution between the 125 Myr and 180 Myr ages of the clusters. Short period rotators in this mass range, however, appear to have spun-down. Bottom: Same as in the top panel, in this case the Pleiades stars have been evolved to the age of M35 using a standard solid-body angular momentum evolution model (e.g. Hartman et al. 2009a). We adopt $K_W = 3.19 \times 10^{47}$ for the wind-constant from Denissenkov et al. (2009), and use the mass-dependent values for the saturation frequency Ω_{sat} from Hartman et al. (2009a). Specifically we use $\Omega_{\text{sat}} = 5.82\Omega_{\odot}$ for $M > 0.99M_{\odot}$, $\Omega_{\text{sat}} = 10.89\Omega_{\odot}$ for $0.86M_{\odot} < M < 0.99M_{\odot}$, $\Omega_{\text{sat}} = 8.70\Omega_{\odot}$ for $0.76M_{\odot} < M < 0.86M_{\odot}$, $\Omega_{\text{sat}} = 4.90\Omega_{\odot}$ for $0.68M_{\odot} < M < 0.76M_{\odot}$, and $\Omega_{\text{sat}} = 2.04\Omega_{\odot}$ for $M < 0.68M_{\odot}$. The lack of evolution between these two clusters is inconsistent with a solid body rotation angular momentum evolution law that is calibrated to the rotation of older clusters and the Sun. Models that allow for decoupling between the rotation of the core and envelope, on the other hand, do predict that the spin-down stalls for the longer period stars at ~ 100 Myr (Bouvier 2008; Denissenkov et al. 2009).

SP-559), Helio- and Asteroseismology: Towards a Golden Future, ed. D. Danesny (Noordwijk: ESA), 341
 Carpenter, J. M. 2001, *AJ*, 121, 2851
 Chabrier, G., Gallardo, J., & Baraffe, I. 2007, *A&A*, 472, L17
 Clarke, D., MacDonald, E. C., & Owens, S. 2004, *A&A*, 415, 677
 Collier Cameron, A., et al. 2009, *MNRAS*, 400, 451
 Deacon, N., & Hambly, N. 2004, *A&A*, 416, 125
 Denissenkov, P. A., Pinsonneault, M., Terndrup, D. M., &

Newsham, G. 2009, *ApJsubmitted*, arXiv:0911.1121
 Fernandez, J., et al. 2009, *ApJ*, 701, 764
 Gray, D. F. 1976, “The Observation and Analysis of Stellar Photospheres”, Wiley & Sons Inc (eds.), New York.
 Haro, G., Chavira, E., & Gonzalez, G. 1982, *Bol. Inst. Tonantzintla*, 3, 1
 Hartman, J. D., Gaudi, B. S., Holman, M. J., McLeod, B. A., Stanek, K. Z., Barranco, J. A., Pinsonneault, M. H.,

- & Kalirai, J. S. 2008, *ApJ*, 675, 1254
- Hartman, J. D., et al. 2009a, *ApJ*, 691, 342
- Hartman, J. D., et al. 2009b, *AJ*, submitted, arXiv:0907.2924
- Høg, E., et al. 2000, *A&A*, 355, L27
- Irwin, J., Hodgkin, S., Aigrain, S., Hebb, L., Bouvier, J., Clarke, C., Moraux, E., & Bramich, D. M. 2007, *MNRAS*, 377, 741
- Irwin, J., Hodgkin, S., Aigrain, S., Bouvier, J., Hebb, L., & Moraux, E. 2008, *MNRAS*, 383, 1588
- Irwin, J., Aigrain, S., Bouvier, J., Hebb, L., Hodgkin, S., Irwin, M., & Moraux, E. 2009, *MNRAS*, 392, 1456
- Irwin, J., & Bouvier, J. 2009, *IAU Symposium*, 258, 363
- Jackson, R. J., Jeffries, R. D., & Maxted, P. F. L. 2009, *MNRAS*, 399, L89
- Jackson, R. J., & Jeffries, R. D. 2010, *MNRAS*, 402, 1380
- James, D. J., et al. 2010, *A&A*, in press, arXiv:1004.0047
- Jeffries, R. D., Jackson, R. J., James, D. J., & Cargile, P. A. 2009, *MNRAS*, 400, 317
- Kalirai, J. S., Fahlman, G. G., Richer, H. B., & Ventura, P. 2003, *AJ*, 126, 1402
- Kawaler, S. D. 1988, *ApJ*, 333, 236
- Kenyon, S. J., & Hartmann, L. 1995, *ApJS*, 101, 117
- Kitchatinov, L. L. 2005, *Phys.-Usp.*, 48, 449
- Königl, A. 1991, *ApJ*, 333, 236
- Kovács, G., Bakos, G., & Noyes, R. W. 2005, *MNRAS*, 356, 557
- Krishnamurthi, A., et al. 1998, *ApJ*, 493, 914
- Lomb, N. R. 1976, *A&SS*, 39, 447
- Mamajek, E. E., & Hillenbrand, L. A. 2008, *ApJ*, 687, 1264
- Marilli, E., Catalano, S., & Frasca, A. 1997, *MmSAI*, 68, 895
- Matt, S., & Pudritz, R. E. 2005, *ApJ*, 632, L135
- Matt, S., & Pudritz, R. E. 2008a, *ApJ*, 678, 1109
- Matt, S., & Pudritz, R. E. 2008b, *ApJ*, 681, 391
- Mazzei, P., & Piggato, L. 1989, *A&A*, 213, L1
- Meibom, S., Mathieu, R. D., & Stassun, K. G. 2009, *ApJ*, 695, 679
- Mermilliod, J. C. 1981, *A&A*, 97, 235
- Messina, S. 2001, *A&A*, 371, 1024
- Monet, D. G., et al. 2003, *AJ*, 125, 984
- Pál, A., & Bakos, G. Á. 2006, *PASP*, 118, 1474
- Pál, A. 2009, Ph.D. Thesis, Eötvös Loránd University, arXiv:0906.3486
- Press, W. H., & Rybicki, G. B. 1989, *ApJ*, 338, 277
- Press, W. H., Teukolsky, S. A., Vetterling, W. T., & Flannery, B. P. 1992, *Numerical Recipes in C*, 2nd ed. (New York: Cambridge University Press)
- Prosser, C. F., Schild, R. E., Stauffer, J. R., & Jones, B. F. 1993a, *PASP*, 105, 269
- Prosser, C. F., et al. 1993b, *PASP*, 105, 1407
- Prosser, C. F., et al. 1995, *PASP*, 107, 211
- Queloz, D., Allain, S., Mermilliod, J.-C., Bouvier, J., & Mayor, M. 1998, *A&A*, 335, 183
- Röser, S., Schilbach, E., Schwan, H., Kharchenko, N. V., Piskunov, A. E., & Scholz, R.-D. 2008, *A&A*, 488, 401
- Samus, N. N., et al. 2003, *Astronomy Letters*, 29, 468
- Scargle, J. D. 1982, *ApJ*, 263, 835
- Schilbach, E., Robichon, N., Souchay, J., & Guibert, J. 1995, *A&A*, 299, 696
- Scholz, A., & Eislöffel, J. 2004, *A&A*, 421, 259
- Schuler, S. C., King, J. R., Fischer, D. A., Soderblom, D. R., & Jones, B. F. 2003, *AJ*, 125, 2085
- Shu, F., Najita, J., Ostriker, E., Wilkin, F., Ruden, S., & Lizano, S. 1994, *ApJ*, 429, 781
- Siess, L., Dufour, E., & Forestini, M. 2000, *A&A*, 358, 593
- Skrutskie, M. F., et al. 2006, *AJ*, 131, 1163
- Skumanich, A. 1972, *ApJ*, 171, 565
- Soderblom, D. R., Stauffer, J. R., Hudon, J. D., & Jones, B. F. 1993, *ApJS*, 85, 315
- Soderblom, D., Nelan, E., Benedict, G., McArthur, B., Ramirez, I., Spiesman, W., & Jones, B. 2005, *AJ*, 129, 161
- Soderblom, D. R., Laskar, T., Valenti, J. A., Stauffer, J. R., & Rebull, L. M. 2009, *AJ*, 138, 1292
- Stauffer, J. R., Schild, R. A., Baliunas, S. L., & Africano, J. L. 1987, *PASP*, 99, 471
- Stauffer, J. R., Schultz, G., & Kirkpatrick, J. D. 1998, *ApJ*, 499, L199
- Stauffer, J. R., Burton, F. J., Backman, D., Hartmann, L. W., Barrado y Navascués, D., Pinsonneault, M. H., Terndrup, D. M., & Muench, A. A. 2003, *AJ*, 126, 833
- Stauffer, J. R., et al. 2007, *ApJS*, 172, 663
- Sukhbold, T., & Howell, S. B. 2009, *PASP*, 121, 1188
- Terndrup, D. M., Krishnamurthi, A., Pinsonneault, M. H., & Stauffer, J. R. 1999, *AJ*, 118, 1814
- Terndrup, D. M., Stauffer, J. R., Pinsonneault, M. H., Sills, A., Yuan, Y., Jones, B. F., Fischer, D., & Krishnamurthi, A. 2000, *AJ*, 119, 1303
- van Leeuwen, F., Alphenaar, P., & Meys, J. J. M. 1987, *A&AS*, 67, 483
- van Leeuwen, F. 2009, *A&A*, 497, 209
- von Braun, K., et al. 2009, *IAU Symposium*, 253, 478
- Walker, G. A. H., et al. 2007, *ApJ*, 659, 1611
- Yee, J. C., & Jensen, E. L. N. 2010, *ApJ*, 711, 303
- Yi, S. K., et al. 2001, *ApJS*, 136, 417

ID	RAdeg J2000	DEdeg J2000	OtherID	Per d	ePer d	fwidth d ⁻¹	rPer	rAmp mag	Bmag mag	Vmag mag	Kmag mag	Mass M_{\odot}	Radius R_{\odot}	vsini km s ⁻¹	rvsini	fbinary
HAT-259-0003751	51.898273	24.528660	DH001	7.26243656	0.00274337	0.00345	...	0.0194	-9.99	-9.99	9.892	0.791	0.692	-99.990000
HAT-214-0002419	52.203186	26.499350	DH007	6.48431835	0.00001564	0.00211	...	0.0203	-9.99	-9.99	9.924	0.783	0.685	-99.990000
HAT-259-0003836	52.639614	26.215767	DH011	4.81593936	0.00030922	0.00227	...	0.0787	-9.99	-9.99	10.279	0.702	0.613	-99.990000
HAT-259-0006363	52.799591	25.165100	DH014	8.03366876	0.00103605	0.00250	...	0.0916	-9.99	-9.99	10.602	0.640	0.561	-99.990000
HAT-259-0009323	52.810955	25.981148	DH015	2.41116752	0.00007308	0.00239	...	0.0590	-9.99	-9.99	11.091	0.551	0.511	-99.990000
HAT-259-0002998	52.824719	26.028849	...	6.37055838	0.00006763	0.00017	...	0.0839	-9.99	-9.99	10.037	0.756	0.660	-99.990000
HAT-214-0001101	52.890076	26.265507	PELS008,AKIII170	3.24215918	0.00016423	0.00242	...	0.0288	11.45	10.77	9.068	1.022	0.921	15.500000	Q98	...
HAT-259-0005281	53.001957	23.774900	PELS109	8.36686239	0.00002128	0.00204	...	0.0601	15.27	13.95	10.520	0.655	0.573	5.500000	Q98	...
HAT-259-0004678	53.214275	25.579544	DH023	2.08690706	0.00003688	0.00256	...	0.0848	-9.99	-9.99	10.323	0.693	0.605	-99.990000
HAT-259-0003433	53.251518	25.996056	DH025	9.07804569	0.00003463	0.00215	...	0.0264	-9.99	-9.99	10.128	0.735	0.642	-99.990000

Table 1. Catalogue of rotation periods for Pleiades stars. The full table includes 383 stars – 368 have periods determined from our photometry, and 15 have periods taken from the literature. We exclude the star HII 3167 with a period listed on WEBDA because it is not a cluster member, and we include the star CFHT-PL-8 which is not included in the S07 catalogue. We also include 4 stars excluded from the S07 catalogue, which have previously been identified as candidate cluster members, and which we found to be probable cluster members in section 3.5, and 14 stars which we have newly determined to be probable cluster members. The former stars are SRS 34337, SRS 79807, HCG 84 and HCG 235, while the latter stars can be identified by having no "OtherID" given. The first ID is an internal HAT-ID and is the ID used for labeling the light curves, the other IDs are defined in S07. The formal error on the period from fitting a Gaussian to the peak in the periodogram is given by ePer. The 1σ width of the Gaussian peak (in frequency) is given by fwidth. Other references with periods for the star in question are given in rPer, the actual periods are given in Table 4. The r -band peak-to-peak amplitude of the light curve is given by rAmp; stars without an amplitude listed have periods taken from the literature. The mass and radius are estimated from the K magnitude and the YY2 isochrones as described in the text, except for 9 faint stars from Scholz & Eislöffel (2004) and 1 faint star from Terndrup et al. (1999) for which the masses and radii are determined using the Baraffe et al. (1998) isochrones. The reference for the $v \sin i$ value is given by rvsini, and fbinary is a flag indicating if the star is a known spectroscopic or visual binary system, it also includes the reference for this determination. Positions and magnitudes are taken from S07. Stars which were not included in the S07 catalogue have positions and magnitudes taken from 2MASS or the 2MASS 6x PSC. For CFHT-PL 8 we take the optical photometry from Samus et al. (2003), for SRS 34337 and SRS 79807 we take the optical photometry from Schilbach et al. (1995), while for HAT-259-0000829 we take the optical photometry from the Tycho-2 catalogue (Høg et al. 2000). The full table is included in the supplementary material of the online edition of the journal. A portion is shown here for guidance regarding its form and content. Abbreviations for the references are defined in the ReadMe file associated with the electronic version of the table.

ID	RAdeg J2000	DEdeg J2000	OtherID	Nobs	RMS mag	Bmag mag	Vmag mag	Kmag mag	Mass M_{\odot}	Radius R_{\odot}	vsini km s ⁻¹	rvsini	fbinary
HAT-259-0000604	51.925262	23.803688	PELS121	6047	0.01314	10.96	10.30	8.679	1.150	1.057	4.900000	Q98	...
HAT-259-0001639	52.168613	25.607782	AKIII59	6020	0.00581	12.59	11.75	9.723	0.832	0.732	-99.990000
HAT-259-0002068	52.409874	24.510546	DH008	6055	0.02236	-9.99	-9.99	9.698	0.839	0.738	-99.990000
HAT-259-0001310	53.274277	22.134232	PELS004,DH026,AKIII131	6046	0.00632	12.25	11.43	9.425	0.911	0.809	2.600000	Q98	...
HAT-259-0010017	53.293736	22.522045	DH027	5983	0.04235	-9.99	-9.99	11.248	0.526	0.502	-99.990000
HAT-259-0000347	53.530495	24.344501	PELS006,TrS4,AKIII288	6035	0.01747	10.08	9.57	8.274	1.309	1.247	35.900000	Q98	...
HAT-259-0004453	53.684944	26.096003	DH037	5977	0.03269	-9.99	-9.99	10.371	0.683	0.597	-99.990000
HAT-259-0000705	53.696770	26.094885	PELS007,AKIII327	6009	0.00490	11.14	10.48	8.833	1.097	1.000	2.700000	Q98	...
HAT-259-0000440	53.882030	22.823627	PELS124	6050	0.01401	10.40	9.86	8.541	1.200	1.115	20.500000	Q98	...
HAT-259-0001134	54.004112	24.266083	AKIII391	6013	0.00495	12.06	11.29	9.388	0.922	0.820	2.300000	Q98	...

Table 2. Catalogue of Pleiades members observed by HATNet without period determinations. The full table includes 120 stars. We include the stars HII 708, HII 727, HII 975, and HHJ 409, which have period measurements taken from the literature, and are included in table 1, but did not have periods recovered from the HATNet light curves. The columns are as in table 1, here we also include Nobs, which is the number of photometric observations, and the unbiased RMS of the HATNet TFA light curve for the target. Only stars with $9.5 < r < 14.5$ are included in this table. The full table is included in the supplementary material of the online edition of the journal. A portion is shown here for guidance regarding its form and content. Abbreviations for the references are defined in the ReadMe file associated with the electronic version of the table.

ID	RAdeg J2000	DEdeg J2000	Per d	rAmp mag	Jmag mag	Hmag mag	Kmag mag
HAT-213-0004432	46.376495	27.295223	1.47490588	0.0421	11.386	11.002	10.921
HAT-213-0000301	46.395025	26.326672	0.49278549	0.0068	7.894	7.317	7.198
HAT-213-0003310	46.423947	26.964050	0.51638485	0.0301	10.947	10.575	10.448
HAT-258-0007599	46.452067	26.214544	0.80443471	0.0680	11.960	11.292	11.068
HAT-258-0001512	46.545842	24.555460	1.56383216	0.0114	10.440	10.123	10.063
HAT-213-0000501	46.549253	26.699934	1.02287839	0.0544	7.864	6.928	6.573
HAT-258-0005170	46.567769	24.944794	7.96319798	0.0110	11.796	11.298	11.198
HAT-213-0005056	46.574536	26.634954	6.48431835	0.0192	11.557	11.194	11.097
HAT-258-0002836	46.593644	24.553173	0.12926165	0.0015	11.035	10.531	10.453
HAT-213-0008723	46.597723	26.747597	0.61090482	0.0228	12.609	12.438	12.416

Table 3. Catalogue of periodic variables in HATNet field G259 that are not cluster members. The full table includes 1804 stars. The positions and magnitudes are taken from 2MASS. The amplitude is the peak-to-peak amplitude of the best-fit sinusoid to the signal-recovery-mode TFA light curve of each star. Note that the true amplitude may be systematically higher by a factor of ~ 1.3 (see section 3.3). The full table is included in the supplementary material of the online edition of the journal. A portion is shown here for guidance regarding its form and content.

ID	Period d	Ref
BPL106	0.170000	S04
BPL115,DH476	0.121250	S04
BPL125,DH494	0.806250	S04
BPL138,DH505	1.075420	S04
BPL150	0.769167	S04
BPL164,DH544	0.840000	S04
CFHT-PL8	0.401000	T71
HCG20,T1B,DH105	2.700000	K98
HCG254,BPL129	0.401667	S04
HCG346,HHJ111,BPL190	1.677920	S04

Table 4. Previous rotation period measurements for Pleiades stars. The full table includes 94 measurements for 66 stars. The full table is included in the supplementary material of the online edition of the journal. A portion is shown here for guidance regarding its form and content. The references are defined in the ReadMe file associated with the electronic version of the table.